Available online at www.sciencedirect.com
ScienceDirect
International Journal of Multiphase Flow 34 (2008) 590–601
International Journal of Multiphase Flow
www.elsevier.com/locate/ijmulflow

# Elongated bubbles in microchannels. Part I: Experimental study and modeling of elongated bubble velocity

Bruno Agostini [1], Rémi Revellin [1], John R. Thome *

*EPFL STI ISE LTCM, ME G1 464, Station 9, CH-1015 Lausanne, Switzerland*

Received 15 February 2007; received in revised form 17 July 2007

**Abstract**

The velocity of elongated vapor bubbles exiting two horizontal micro-evaporator channels with refrigerant R-134a was studied. Experiments with tube diameters of 509 and 790 μm, mass velocities from 200 to 1500 kg/m$^2$ s, vapor qualities from 2% to 19% and a nominal saturation temperature of 30 °C were analyzed with a fast, high-definition digital video camera. It was found from image processing of numerous videos that the elongated bubble velocity relative to that of homogeneous flow increased with increasing bubble length until a plateau was reached, and also increased with increasing channel diameter and increasing mass velocity. Furthermore an analytical model developed for a diabatic two-phase flow, has been proposed that is able to predict these trends. In addition, the model shows that the relative elongated bubble velocity should decrease with increasing pressure, which is consistent with the physics of two-phase flow.


*Keywords:* Microchannels; Bubble collision; Two-phase flow; Velocity; Elongated bubble

## 1. Introduction

Slug flow is one of the basic vapor–liquid flow patterns which takes place inside microchannels. It occurs over a wide range of flow parameters. It is characterized by an alternating succession of elongated bubbles and liquid slugs. Many interactions between elongated bubbles may occur, among them bubble collision. Collision of elongated bubbles in microchannels is a one-dimensional phenomenon because of the confinement of the small channel and has been observed experimentally by Revellin et al. (2006), where it was identified as one of the most important parameters influencing flow pattern transition (for example, refer to the diabatic flow pattern map proposed by Revellin and Thome (2006)).

Many studies have already been carried out on measuring void fractions in conventional channels and numerous models already exist. Among them, the homogeneous model is based on the assumption that the vapor and liquid phases flow at the same average velocities. Zuber and Findlay (1965) proposed a general form of the drift flux model, which takes into account both the effect of nonuniform velocity and void profiles as well as the effect of the local relative velocity between the phases. The first effect is taken into account by a distribution parameter, whereas the weighted average drift velocity accounts for the latter. However, these two models do not take into account the influence of bubble length on its velocity, i.e. the individual characteristics of the flow.

The length of Taylor bubbles has been studied by Barnea and Taitel (1993), who proposed a model for slug distribution in gas–liquid slug flow. Their model assumes a random distribution of bubble lengths at the inlet of the channel and it calculates the increase or decrease in each individual slug's length, including the disappearance of the short slugs, as they move downstream. The slug length distribution in the developed region seems to follow approximately a log normal distribution. Cook and Behnia

* Corresponding author. Tel.: +41 21 693 5981; fax: +41 21 693 5960.
*E-mail address:* john.thome@epfl.ch (J.R. Thome).
[1] Co-authors.

0301-9322/$ - see front matter © 2007 Elsevier Ltd. All rights reserved.
doi:10.1016/j.ijmultiphaseflow.2007.07.007

(2000) proposed a slug length prediction in nearly horizontal gas–liquid intermittent flow. Their data showed that all the turbulent flow results could be correlated by the same expression regardless of the value of the slug liquid Reynolds number.

Bubble collision has been studied by many authors but most of the time for gas–liquid flow in vertical macrochannels and seldom in horizontal ones. Talvy et al. (2000) observed the interaction between two consecutive elongated bubbles in a vertical pipe. They experimentally found that the trailing bubble did not affect the motion of the leading one and that the trailing bubble, on the other hand, was sensitive to the velocity distortion in the wake of the leading bubble. In fact, they showed that the acceleration of the trailing bubble is quite significant in the near wake region just behind of the leading elongated bubble. Pinto et al. (1998) studied the collision of two gas slugs rising in a co-current flowing liquid in vertical tubes of 22, 32 and 52 mm internal diameter. Generally they found that the minimum distance between slugs above which there is no interaction is about 5*D* in the turbulent liquid flow regime and 10*D* in the laminar liquid flow regime (some other behaviors were also observed).

In summary, several studies exist on measurement and prediction of the elongated bubble velocity, length and bubble collision but all of them for gas–liquid flow in macrochannels. The influence of bubble length on bubble velocity has apparently not yet been studied for two-phase flow in microchannels. In this paper, new experimental observations of this phenomena are presented as well as relative bubble velocity and bubble length measurements and a new model developed for a diabatic two-phase flow is proposed to predict their relationship.

## 2. Description of the test facility

The microchannel test facility is described in detail in Revellin (2005). The test facility was designed to operate using either a speed controlled micropump, or the pressure difference between two temperature-controlled reservoirs (the latter mode was used for all the present tests and is presented in Fig. 1). A valve installed between the upstream reservoir and the test section is used to avoid flow oscillations in the loop and a wide range of stable operating conditions is thus achieved.

### 2.1. Test section

The test section consisted of four subsections: (i) an 80 mm long, thin wall stainless steel tube used as a preheater, (ii) a 20 mm long plastic (PEEK) tube for electrical insulation, (iii) a 110 mm long stainless steel tube microevaporator and (iv) a 100 mm long glass tube for flow pattern visualization and pressure drop measurements, as shown in Fig. 2. Two copper clamps were attached to both the preheater and the evaporator and heating was provided by two Sorensen DC power supplies. Two pressure transducers were installed at the inlet and outlet of the test section and two 0.25 mm thermocouples were placed in the fluid at the same locations. Four 0.25 mm thermocouples were also attached on the external surface of the sight glass tubes (before the inlet and after the outlet of both the preheater and the evaporator) to measure local fluid saturation temperatures. Two more 0.25 mm thermocouples were installed on the two heated tubes to avoid exceeding the critical heat flux. All the test section was thermally insulated. Careful attention was made to match up the ends of

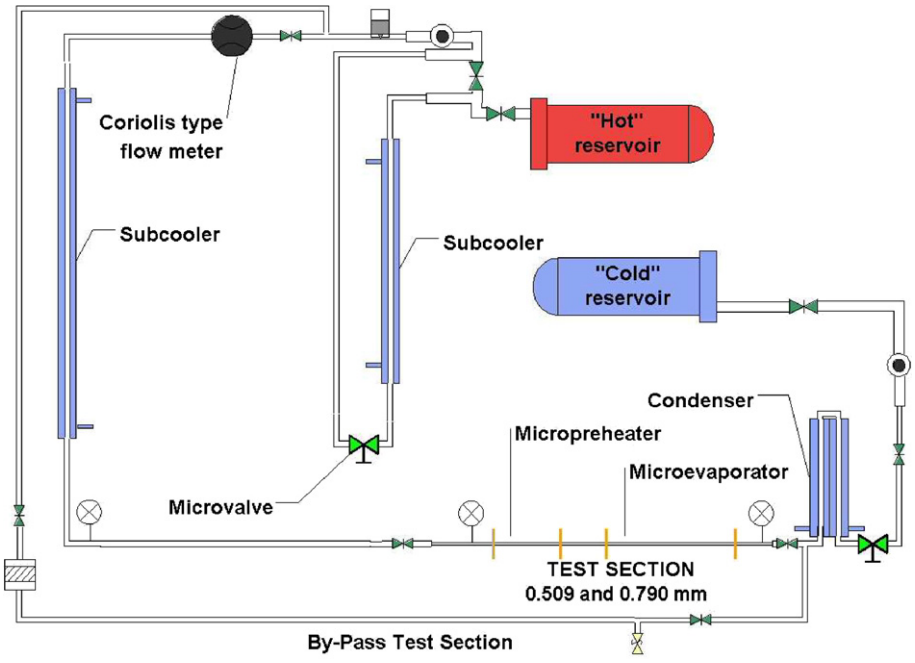


Fig. 1. Schematic of the test loop.

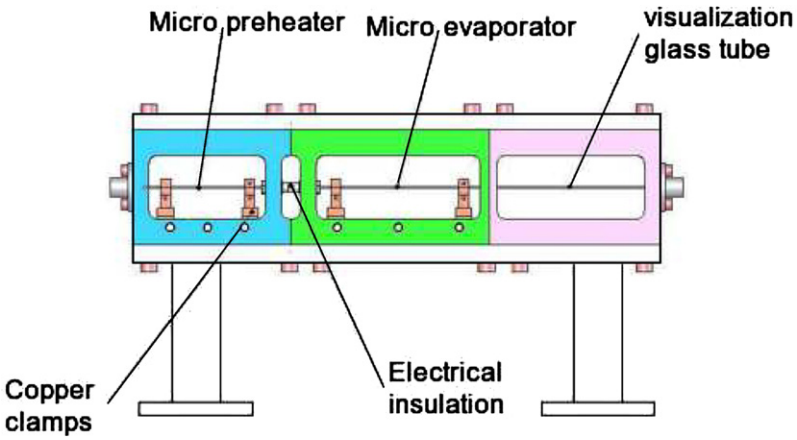


Fig. 2. Schematic diagram of the test section: front view.

the glass and stainless steel tubes. The adiabatic zone after the micro-evaporator was 120 mm long.

### 2.2. Measurements and accuracy

A Coriolis mass flow meter was used to measure the flow rate of the subcooled refrigerant (±0.1%). The amount of Joule heating was determined by measuring the DC voltage (±0.02%) and the current by a DC current transformer (±3.5% for low currents and ±1% for high ones). The absolute pressure transducers for monitoring the local pressures were accurate to ±5 mbar and the thermocouples to ±0.1 °C, according to their calibrations. The vapor quality entering the flow visualization tube was estimated to be accurate to ±5.6% of the value for most test conditions, e.g. ±0.0056 of a vapor quality of 0.10.

The total database from this study covers one refrigerant (R-134a) and two tube diameters (509 and 790 μm). The micro-evaporator heated length was 70.7 mm and the inlet subcooling to the micro-evaporator was 3 °C. The mass fluxes ranged from 200 to 1500 kg/m$^2$ s and the heat fluxes that produced the two-phase flow ranged from 6.5 to 31.8 kW/m$^2$. The saturation temperature tested here was about 30 °C. Experimental conditions and uncertainties are summarized in Table 1 with $D$ the tube diameter, $e/D$ the relative surface roughness of the glass tube, $L_{MEV}$ the length of the micro-evaporator, $G$ the mass velocity, $q$ the heat flux, $T_{sat}$ the saturation temperature, $P_{sat}$ the saturation pressure, $\Delta T_{sub}$ the inlet subcooling, $x_{MEV,out}$ the vapor quality at outlet of the micro-evaporator, $U_G$ the vapor velocity and $U_h$ the homogeneous velocity.

Notably, the present setup involves actual vapor–liquid two-phase flows exiting a micro-evaporator channel. The bubbles and subsequent flow regimes observed here originated from nucleation in the evaporator, just like in a microchannel cooling element attached to a computer chip, for instance. Thus, here the resulting flow pattern and bubble characteristics are produced by the boiling process itself, not the hydrodynamics of an injector, mixer or header used in adiabatic tests. Furthermore, compared to most of the macroscale studies done with air and water, the surface tension of R134a is about an order of magnitude lower.

Table 1
Experimental conditions and uncertainties

| Parameter | Values | Uncertainties | Units |
|---|---|---|---|
| Fluid | R-134 | – | – |
| $D$ | 509, 790 | ±1% | μm |
| $\frac{e}{D}$ | < 0.002% | – | – |
| $L_{MEV}$ | 70.7 | < 2.5% | mm |
| $G$ | 200–1500 | ±2% | kg/m$^2$ s |
| $q$ | 6.5–31.8 | < 5.7% | kW/m$^2$ |
| $T_{sat}$ | 30 | ±0.1 | °C |
| $P_{sat}$ | 7.7 | < 0.07% | bar |
| $\Delta T_{sub}$ | 3 | ±0.1 | °C |
| $x_{MEV,out}$ | 0.02–0.19 | 5.6% | – |
| $U_G$ | 0.39–4.38 | 0.2–2.6% | m/s |
| $U_h$ | 0.39–3.3 | <7.25% | m/s |

## 3. Experimental results

Thirty-six videos have been recorded for different experimental conditions for which a multiple train of sequential bubbles was observed, and summarized in Table 1, using a high-speed high-definition video camera (FASTCAM, 120,000 frames per second maximum). The images were taken at 10,000 frames per second with a shutter time down to 20 μs with 256 × 512 pixels per images. The video camera was located after the micro-evaporator facing the glass tube. Each video sequence is composed of 2000 images for a total time of 0.2 s. In order to determine the length and velocity of each vapor bubble, an image processing software has been developed that applied the following procedure:

(i) as shown in Fig. 3a, a contrast and light normalization was applied to each of the 2000 images for every video,
(ii) as shown in Fig. 3b, a threshold was applied to each image so that only the outline of the bubbles was visible, and

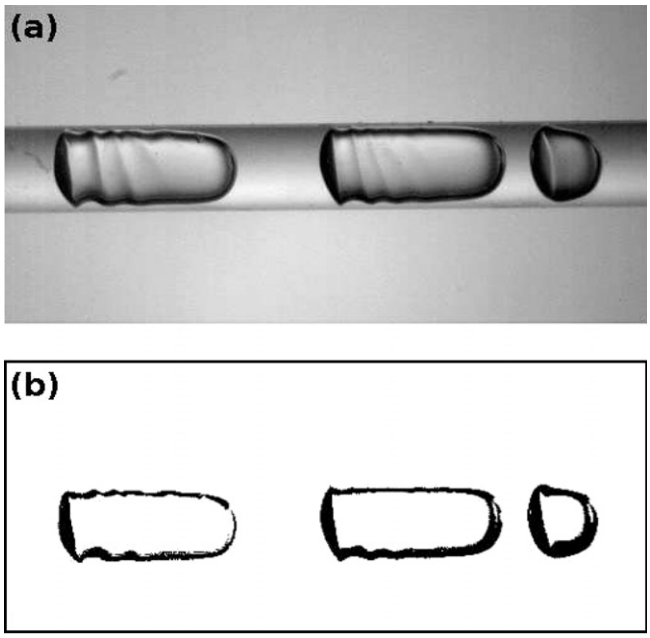


Fig. 3. Image of elongated bubble flow: (a) after contrast and light normalization and (b) after threshold was applied.

(iii) an edge detection algorithm was applied to the middle longitudinal line (from left to right) of each image giving the position of the front and back of each bubble, as shown in Fig. 4.

(iv) each edge was identified as the front or back of a bubble using the light intensity profile on a transverse line (from top to bottom) of the original image shown in Fig. 3a. As shown in Fig. 5, the presence of liquid or vapor between two edges can be identified with the shape of the light intensity profile.

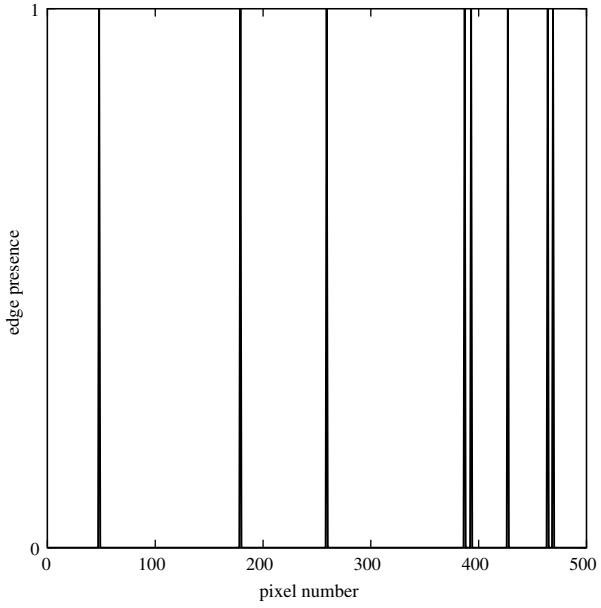


Fig. 4. Edge detection applied on the middle line of an image of elongated bubble flow.

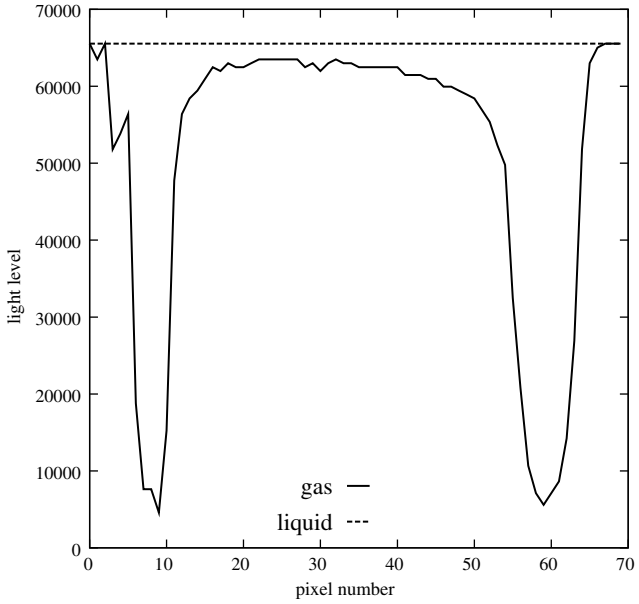


Fig. 5. Gray level profile applied on a transverse line of an image of elongated bubble flow indicating a bubble is present at this location.

Finally, for each of the 2000 images of the 36 videos, the positions of the front and back of every elongated bubble on the videos were obtained. The resolution of the method can be estimated using Fig. 4: the fourth and sixth edge are doubled because of artifacts on the videos so that the uncertainty on the position of the edges is about $\Delta p = \pm 3$ pixels.

To calculate the elongated bubble velocities as a function of their length, the following procedure was applied to each elongated bubble in the flow:

(v) the frame number when the elongated bubble front appears and disappears on the video are, respectively $f_i$ and $f_o$. The pixel position of the bubble front when the elongated bubble front appears and disappears on the video are, respectively $p_i$ and $p_o$. Then the elongated bubble velocity is:

$$U_G = (p_o - p_i) \cdot S \cdot F/(f_o - f_i) \quad (1)$$

$S$ and $F$ being respectively the image scale (18.248 μm/pixel) and the frame rate (10,000 images per second),

(vi) if the elongated bubble length is smaller than the image width, the pixel position of the front and back of the elongated bubble in the frame $f_o$ are, respectively $p_{f,o}$ and $p_{b,o}$. Then the bubble length is

$$L_G = (p_{f,o} - p_{b,o}) \cdot S \quad (2)$$

(vii) if the elongated bubble length is longer than the image width, the frame number when the elongated bubble back appears on the video is $f_{b,i}$, the frame number when the elongated bubble front disappears on the video is $f_{f,o}$. Then the bubble length is

$$L_G = U_G \cdot (f_{f,o} - f_{b,i})/F \quad (3)$$

(viii) finally the uncertainties were calculated with

$$\Delta U_G/U_G = \Delta(p_o - p_i)/(p_o - p_i) = 2\Delta p/(p_o - p_i), \quad (4)$$

$$\Delta L_G/L_G = 2\Delta p/(p_{f,o} - p_{b,o}) \quad (5)$$

if the elongated bubble length is smaller than the image width, and

$$\Delta L_G/L_G = \Delta U_G/U_G \quad (6)$$

if the elongated bubble length is larger than the image width.

In order to eliminate the effect of the average velocity of the flow on the elongated bubble velocity, it seemed logical to substract the homogeneous velocity to obtain the relative elongated bubble velocity. The homogeneous velocity was calculated as follows

$$U_h = \frac{G \cdot x}{\rho_G} + \frac{G \cdot (1-x)}{\rho_L} \quad (7)$$

where $G$, $x$, $\rho_L$ and $\rho_G$ are, respectively the mass velocity, vapor thermodynamic quality, liquid density and vapor density. Indeed, according to the homogeneous model for a horizontal flow, when a flow is composed of small bubbles dispersed in a liquid flow both vapor and liquid travel at the same velocity: the homogeneous velocity. Thus the relative elongated bubble velocity $U_G - U_h$ should tend towards 0 when $L_G \to 0$.

Fig. 6 shows the relative elongated bubble velocities plotted versus bubble length for $D = 500\,\mu m$ and $G = 500\,kg/m^2\,s$, with uncertainties on both $U_G - U_h$ and $L_G$. The elongated bubble relative velocity is clearly a function of the bubble length with a large increase for $0 < L_G < 30\,mm$ and, as expected, tends to 0 when $L_G = 0$. Furthermore $U_G - U_h$ reaches a more or less constant value of 0.7 m/s for $L_G > 30$ mm. Thus, $U_G - U_h$ can be as high as 40% of $U_h$, which is far from being negligible.

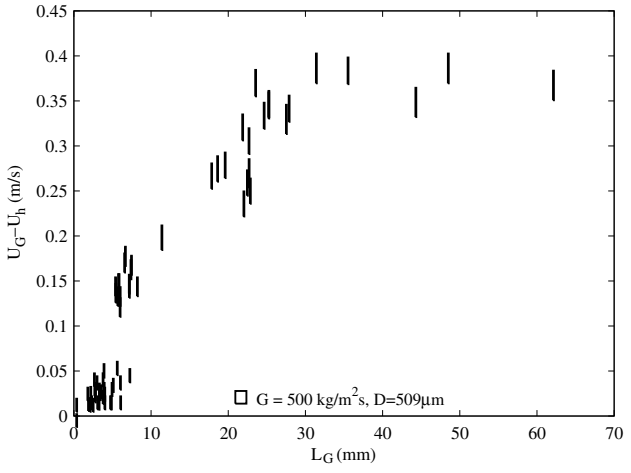


Fig. 6. Relative elongated bubble velocity versus bubble length, with uncertainty bars shown for velocity.

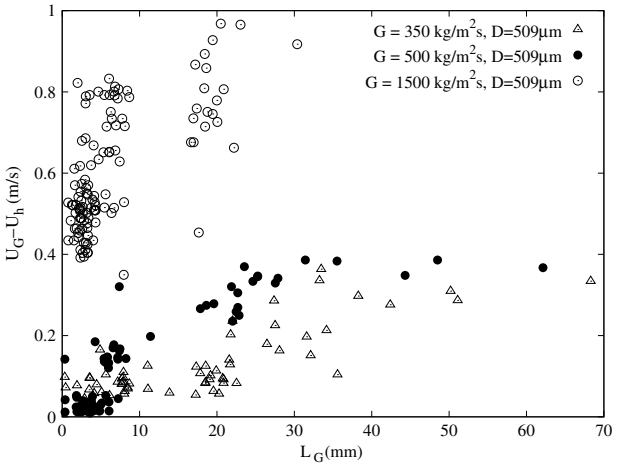


Fig. 7. Relative elongated bubble velocity versus bubble length, for $D = 509$ µm and different mass velocities.

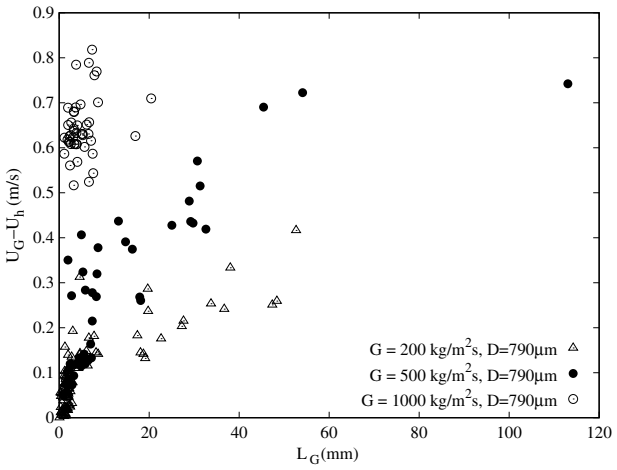


Fig. 8. Relative elongated bubble velocity versus bubble length, for $D = 790$ µm and different mass velocities.

Figs. 7 and 8 show $U_G - U_h$ as a function of $L_G$ for all the videos (two tube diameters and five mass velocities). There is an increase in the dispersion of the data at the higher mass velocities because the transition towards churn flow begins and the elongated bubbles do not have a regular shape anymore. However, the relative elongated bubble velocity is clearly seen to be a function of the mass velocity for a given $L_G$. The following trends can be discerned from Figs. 7 and 8:

- the relative elongated bubble velocity increases with the bubble length,
- for a given $L_G$ the relative elongated bubble velocity increases with $G$,
- the relative elongated bubble velocity seems to increase faster with $L_G$ for higher $G$,
- the relative elongated bubble velocity increases with diameter for a given $G$ and $L_G$.

As noted earlier in the literature review, it is widely accepted that the wake behind a bubble can affect the

velocity of another bubble behind. In order to check if such an effect occurred here, Fig. 9 shows the individual relative elongated bubble velocities plotted as a function of the ratio $L_L/D$, $L_L$ being the length of the liquid slug immediately ahead of the bubble. There seems to be no obvious relationship of $U_G - U_h$ with $L_L/D$, that is confirmed by the low coefficient of correlation $R^2 = 0.23$. Most literature studies show an influence of the liquid slug length on the trailing bubble velocity, which is contradictory with the present results. Several observations can explain this discrepancy:

- In the present study most of the liquid slugs have an $L_L/D$ of around 3–10 and the bubbles have $L_G/D$ ratios much larger than those in macrochannels with values over 100 in some cases,
- In a microtube the liquid layer around the elongated bubbles is much thinner than in a macrotube so that the wake structure behind the leading bubble is probably notably different, thus changing the way the trailing bubble velocity can be influenced by the leading bubble, and
- The elongated bubbles of the present study have been generated by a nucleation process along an evaporator, which is very different from a gas–liquid mixing device. Thus the acceleration given to the bubbles in the evaporator might be prominent on any wake effect.

From Fig. 9 it can be concluded that:

- $L_G$ is indeed the relevant parameter to study the increase of $U_G - U_h$ and
- the elongated bubble and liquid slug lengths are not correlated.

Based on these results, a model has been developed to predict the relationship between $U_G - U_h$ and $L_G$ and is presented in the next section.

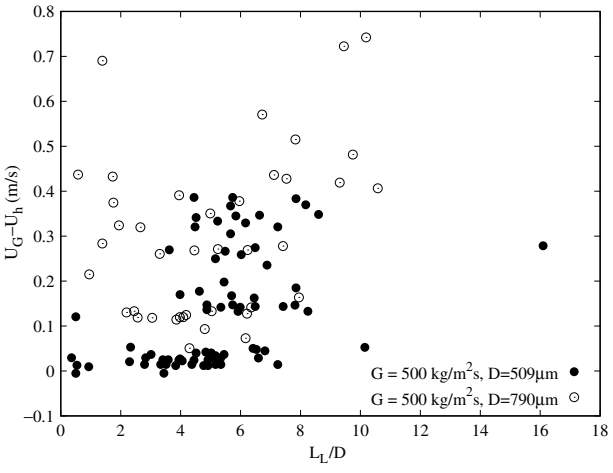


Fig. 9. Relative elongated bubble velocity versus liquid slug length to diameter ratio, for $D = 509$ μm and $D = 790$ μm.

## 4. Description of the model

The model, developed for a diabatic two-phase flow, consists of the determination of the vapor bubble velocity as a function of its length, using equations for the conservation of mass, energy and momentum. Consider a transient two-phase slug flow regime in a round tube of diameter $D$ and cross-sectional area $A$ along a longitudinal $z$-axis at a mass velocity $G$ that is heated uniformly with a constant heat flux $q$. We can consider an elongated bubble of vapor mass flow rate $\dot{m}_G$, vapor velocity $U_G$, vapor density $\rho_G$ and cross-sectional area $A_G$. The control volume considered here is the bubble itself, so that $dz$ refers for a bubble length increment. From continuity we get:

$$\dot{m}_G = A \cdot G \cdot x \tag{8}$$

Differentiating (8) with respect to the channel length $z$ gives

$$\frac{d}{dz}(A_G \cdot U_G \cdot \rho_G) = A \cdot G \cdot \frac{dx}{dz} \tag{9}$$

hence

$$\frac{d}{dz}\left(\frac{A_G}{A} \cdot U_G\right)\rho_G + \left(\frac{A_G}{A} \cdot U_G\right)\frac{d\rho_G}{dz} = G \cdot \frac{dx}{dz} \tag{10}$$

and

$$\frac{d}{dz}\left(\frac{A_G}{A} \cdot U_G\right) = -\frac{A_G}{A} \cdot \frac{U_G}{\rho_G} \cdot \frac{d\rho_G}{dp} \cdot \frac{dp}{dz} + \frac{G}{\rho_G} \cdot \frac{dx}{dz} \tag{11}$$

The product $(A_G/A) \cdot (U_G/\rho_G) \cdot (d\rho_G/dp) \cdot (dp/dz)$ is negligible compared to the product of $(G/\rho_G) \cdot (dx/dz)$. As an example, the calculation performed for the following experimental conditions: $G = 500$ kg/m$^2$ s, $P_{sat} = 7.7$ bar, $q = 15$ kW/m$^2$, $D = 509$ μm, $A_G/A \simeq 1$, $dP/dz = 0.86$ bar/m (for the entire length of the tube) and $U_G = 1.43$ m/s gives $(G/\rho_G) \cdot (dx/dz) \simeq 16.5$ s$^{-1}$ and $(A_G/A) \cdot (U_G/\rho_G) \cdot (d\rho_G/dp) \cdot (dp/dz) \simeq 0.165$ s$^{-1}$. Consequently,

$$\frac{d}{dz}\left[\frac{\pi\left(\frac{D}{2} - \delta\right)^2}{\pi\frac{D^2}{4}} \cdot U_G\right] = \gamma \tag{12}$$

where $\delta$ is the liquid film thickness trapped between the wall and the vapor bubble and

$$\gamma = \frac{4q}{D \cdot h_{LG} \cdot \rho_G} \tag{13}$$

with $h_{LG}$ the latent heat of vaporization while $q$ is the uniform heat flux applied to the micro-evaporator and thus yields the enthalpy absorbed by the bubbles assuming no superheating of the liquid slugs. Rearranging (12), we obtain

$$-\frac{4}{D} \cdot U_G \cdot \frac{d\delta}{dz} + \left(1 - \frac{2\delta}{D}\right)\frac{dU_G}{dz} = \frac{\gamma}{1 - \frac{2\delta}{D}} \tag{14}$$

Furthermore, in Thome et al. (2004) it has been demonstrated that $\delta/D \simeq 1/100$, and we can thus assume that $(1 - 2\delta/D) \simeq 1$. The expression thus reduces to

$$-\frac{4}{D}\cdot U_G\cdot\frac{d\delta}{dz}+\frac{dU_G}{dz}=\gamma \tag{15}$$

From continuity we know also that at a certain cross section of the tube:

$$\dot{m}=cte=\dot{m}_L+\dot{m}_G \tag{16}$$

where $\dot{m}$, $\dot{m}_L$ and $\dot{m}_G$ are, respectively the total, liquid and vapor mass flow rate. Writing (16) in terms of the above variables, it becomes

$$\pi\cdot\frac{D^2}{4}\cdot G=\pi\cdot D\cdot\delta\cdot\rho_L\cdot U_\delta+\pi\left(\frac{D}{2}-\delta\right)^2\rho_G\cdot U_G \tag{17}$$

and finally

$$\frac{4\delta}{D}\cdot\rho_L\cdot U_\delta+\rho_G\cdot U_G=G \tag{18}$$

Differentiating expression (18) for a steady state flow rate, we obtain

$$\frac{4}{D}\cdot\rho_L\cdot U_\delta\cdot\frac{d\delta}{dz}+\frac{4\delta}{D}\cdot\rho_L\cdot\frac{dU_\delta}{dz}+\rho_G\cdot\frac{dU_G}{dz}=\frac{dG}{dz}=0 \tag{19}$$

The variation of the liquid film velocity is assumed to be negligible and by consequence we can say that

$$\frac{4}{D}\cdot\frac{d\delta}{dz}=-\frac{\rho_G}{\rho_L}\cdot\frac{1}{U_\delta}\cdot\frac{dU_G}{dz} \tag{20}$$

From (15) and (20) we get

$$\frac{\rho_G}{\rho_L}\cdot\frac{U_G}{U_\delta}\cdot\frac{dU_G}{dz}+\frac{dU_G}{dz}=\gamma \tag{21}$$

and it follows that

$$\frac{dU_G}{dz}=\frac{\gamma}{1+\frac{U_G}{U_\delta}\cdot\frac{\rho_G}{\rho_L}}=\varphi \tag{22}$$

or

$$\varphi=\frac{\gamma}{1+\frac{G_G}{G_\delta}} \tag{23}$$

where $G_G$ is the mass velocity of the vapor and $G_\delta$ the mass velocity of the liquid film. $G_G/G_\delta$ can be considered as a pseudo slip ratio between the vapor in the bubble and the liquid film surrounding the bubble. For an elongated bubble confined in a microchannel, the average velocity in the liquid layer confined between the bubble and the wall has to be negative because the bubbles travel faster than the liquid slug ahead so that some liquid has to be evacuated by the liquid layer around the bubble, such that $G_\delta<0$. This is illustrated in Fig. 10. The grayed rectangle in the upper part of the figure is the volume of liquid that will disappear during a time interval $\Delta t$ because the bubble is traveling faster than the liquid slug ahead. Furthermore, Kashid et al. (2005) have shown by PIV experiments that recirculation occurs within the liquid slug as illustrated in Fig. 10, that causes a negative velocity at the beginning of the liquid layer, just around the nose of the bubble. This fact and the examination of the upper part of Fig. 10 show that the liquid of the grayed rectangle has to be evacuated by the liquid layer whose average liquid velocity is then necessarily negative. The lower part of Fig. 10 shows how the velocity profile should look like in the liquid layer in order to obtain a negative average velocity. So far no study has been found in the literature on the velocity pro-

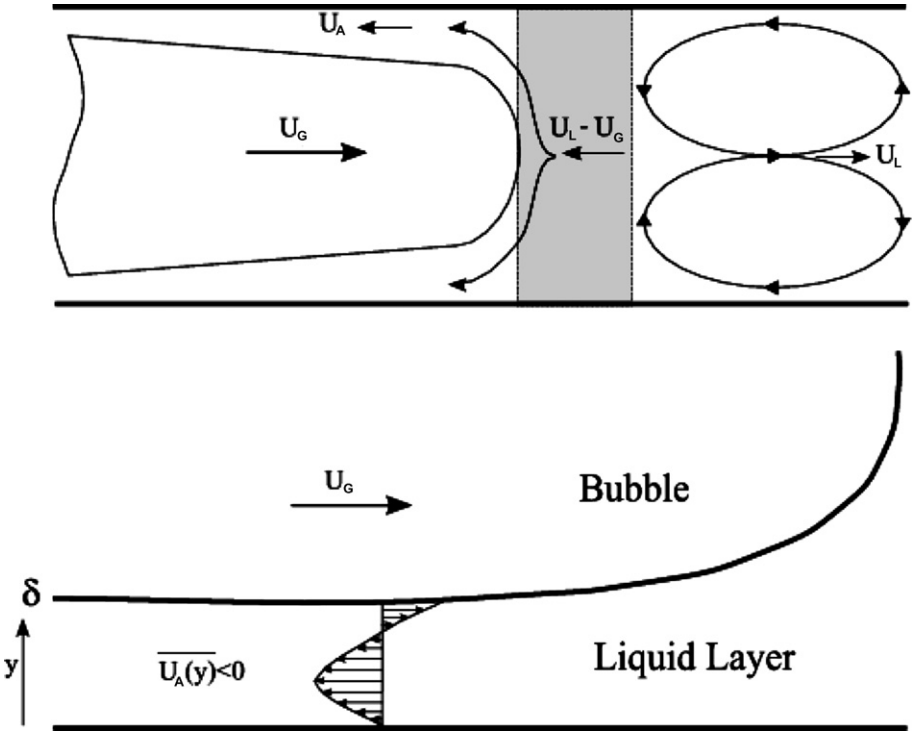


Fig. 10. Schematics of the hypothetical velocity profile in the liquid layer trapped between an elongated bubble and the channel wall.

file in the liquid layer trapped by elongated bubbles in horizontal microchannels so that this question is still unresolved but Fig. 10 seems to be a reasonable conclusion.

Yang et al. (2002) showed in their study that the liquid film thickness was only a function of the Bond number. The Bond number is related to the Confinement number by $\mathrm{Co} = \mathrm{Bo}^{-1/2}$. Since $G_G/G_\delta$ varies proportionally to $\delta/D$ for a constant mass flow, we can assume that $G_G/G_\delta$ is proportional to $C/\mathrm{Co}$ where the constant $C$ is negative. Co is given by the following relation, according to Kew and Cornwell (1997):

$$\mathrm{Co} = \left(\frac{g(\rho_L - \rho_G)D^2}{\sigma}\right)^{-1/2} \tag{24}$$

with $\sigma$ the surface tension and $g$ the acceleration of gravity. Thus, we obtain the following expression for $\varphi$:

$$\frac{dU_G}{dz} = \varphi = \frac{\gamma}{1 + \frac{C}{\mathrm{Co}}} \tag{25}$$

After integration of expression (25), it becomes

$$U_G = \varphi \cdot L_G + U_h \tag{26}$$

where $U_h$ is the homogeneous velocity. This equation gives an increase in bubble velocity with bubble length, which should be equal to the bubble velocity only if friction is negligible therefore this equation is appropriate for short vapor bubbles. However, if the bubbles are longer, we have to take into account the effect of friction in the momentum equation, which is done below.

Now consider a vapor bubble of surface area $S_G$, mass $M_G$, volume $V_G$ and vapor density $\rho_G$. Ribatski et al. (2006) showed in their analysis of experimental data and prediction methods for two-phase frictional pressure drop in microchannels that the homogeneous model was one of the most accurate prediction methods. As a result, it is reasonable to calculate the pressure drop gradient with the homogeneous model and thus use $U_h$ (homogeneous velocity at the outlet of the evaporator) as a reference velocity. Let us write the transient expression for the conservation of momentum for an elongated bubble flowing at $U_G(z,t)$

$$M_G \cdot \frac{dU_G}{dt} = M_G \cdot U_G \cdot \frac{dU_G}{dz} - \frac{1}{2} \cdot f_i \cdot \rho_G \cdot S_G \cdot U_G^2 + V_G \cdot \frac{dp}{dz}. \tag{27}$$

As a first approximation, the term $dU_G/dz$ is calculated with Eq. (25)

$$\frac{dU_G}{dz} = \varphi \tag{28}$$

and the homogeneous pressure gradient is

$$V_G \cdot \frac{dp}{dz} = -M_G \cdot U_h \cdot \varphi + \frac{1}{2} \cdot f_i \cdot \rho_G \cdot S_G \cdot U_h^2 \tag{29}$$

so that Eq. (27) can be written

$$M_G \cdot \frac{dU_G}{dt} = M_G \cdot U_G \cdot \varphi - \frac{1}{2} \cdot f_i \cdot \rho_G \cdot S_G \cdot U_G^2 - M_G \cdot U_h \cdot \varphi + \frac{1}{2} \cdot f_i \cdot \rho_G \cdot S_G \cdot U_h^2. \tag{30}$$

Noticing that $dU_h/dt = 0$ and supposing that $U_G \cdot U_h \approx U_h^2$, rearranging yields

$$M_G \cdot \frac{dU^*}{dt} = M_G \cdot U^* \cdot \varphi - \frac{1}{2} \cdot f_i \cdot \rho_G \cdot S_G \cdot U^{*2} \tag{31}$$

with $U^* = U_G - U_h$. Eq. (31) simply states that during the acceleration of the bubble due to evaporation, a part of the friction force counterbalances this acceleration until an equilibrium velocity is reached.

It is of importance to emphasize here that the interfacial friction factor $f_i$ is expressed using $U_G$. The interfacial friction factor is originally formulated with $U_G - U_\delta$ but $U_\delta$ (the liquid layer velocity) is neglected here. $f_i$ is expressed with the following conventional relations:

$$f_i = 64 \cdot Re_G^{-1} \quad \text{for} \quad Re_G \leqslant 2000 \tag{32}$$

$$f_i = 0.316 \cdot Re_G^{-0.25} \quad \text{for} \quad Re_G > 2000 \tag{33}$$

with the vapor Reynolds number expressed as

$$Re_G = \frac{\rho_G \cdot U_G \cdot D}{\mu_G} \tag{34}$$

Substituting and rearranging (31) it becomes

$$\frac{dU^*}{dt} = U^* \cdot \varphi \left(1 - \frac{f_i \cdot \rho_G \cdot S_G}{2 \cdot M_G \cdot \varphi} \cdot U^*\right) \tag{35}$$

Furthermore, $dz/dt = U^*$ thus

$$\frac{dU^*}{dz} = \varphi(1 - \beta \cdot U^*) \quad \text{with} \quad \beta = \frac{f_i \cdot \rho_G \cdot S_G}{2 \cdot M_G \cdot \varphi} \tag{36}$$

If the elongated bubble is considered as a cylinder of diameter $D$ (Thome et al. (2004) showed that $\delta \ll D$ so the liquid film thickness can be neglected) and a length $L_G$, $\beta$ is then expressed as

$$\beta = \frac{2 f_i}{D \cdot \varphi} \tag{37}$$

Eq. (36) is integrated as follows:

$$-\frac{1}{\beta} \ln(1 - \beta \cdot U^*) = \varphi \cdot L_G + A_1 \tag{38}$$

Since $U^* = 0$ at $t = 0$, $L_G = 0$ and thus $A_1 = 0$ and we obtain

$$\ln(1 - \beta \cdot U^*) = -\beta \cdot \varphi \cdot L_G \tag{39}$$

The final solution of $U_G$ is

$$U_G = \frac{1 - \exp(-\varphi \cdot \beta \cdot L_G)}{\beta} + U_h \tag{40}$$

which gives the relationship between the length of a vapor bubble and its velocity. If we express (40) with all the parameters involved, we get

$$U_G = \frac{D \cdot \gamma}{1 + \frac{C}{Co}} \frac{1 - \exp\left(\frac{-2 \cdot f_i \cdot L_G}{D}\right)}{2 \cdot f_i} + U_h \quad (41)$$

The optimization of the model by the least squared method using the present database leads to $C = -0.58$. From Eq. (25) we know that $U_\delta = (U_G \cdot \rho_G \cdot Co)/(C \cdot \rho_L) \simeq U_G/20$. This confirms the assumption $U_G - U_\delta \simeq U_G$ used in writing Eq. (31).

Regarding Eq. (41), there is a singularity for $Co = 0.58$. This limit almost corresponds to the limit of Cornwell and Kew (1995) who proposed a value of $Co = 0.5$ as the transition threshold between confined and non-confined bubble flow (taken as a tentative threshold between macroscale and microscale two-phase flow). They showed that the confinement was significant if the Confinement number was greater than 0.5. In the present study, the model works as long as $Co > 0.58$. In this case the velocity of the liquid film trapped between the wall and the vapor bubble is negative and the channel is a microchannel. When $Co \leqslant 0.58$, the confinement effect is negligible, stratification occurs and the assumption of the negative velocity of the liquid film is no more valid and the velocity becomes positive. However, the choice of the value 0.5 was based on a limited number of observations by Cornwell and Kew and hence this threshold can be considered to be a qualitative value rather than a definitive value. The Confinement number (Co) is also related to the Eotvos number (Eo) by the relation $Co = Eo^{-1/2}$. Ullman and Brauner (2006) proposed the threshold for microchannels to be for $Eo < 1.6$ or $Co > 0.79$. The value of 0.58 calculated here thus falls between the Cornwell and Kew (1995)and Ullman and Brauner (2006) thresholds.

The different assumptions used for the model are summarized below:

- uniform and constant heat flux $q$ to generate the vapor bubbles,
- the homogeneous model can be used to calculate the pressure gradient,
- $U_G$ is close to $U_h$,
- $\delta \ll D$,
- $dU_\delta/dz$ is negligible, and
- $U_G - U_\delta \simeq U_G$ for the interfacial friction factor formulation.

## 5. Comparison with experimental data

Fig. 11 shows the comparison between the 484 experimental data points obtained at the exit of a micro-evaporator channel and the model for the conditions summarized in Table 1. All together 90% of the data are predicted within a ±20% error band. The mean absolute error is MAE = 8.9% and the mean error is ME = 6.8%. The definitions of MAE and ME are given by Eqs. (42) and (43). The model slightly under-predicts the data but the agreement remains very good.

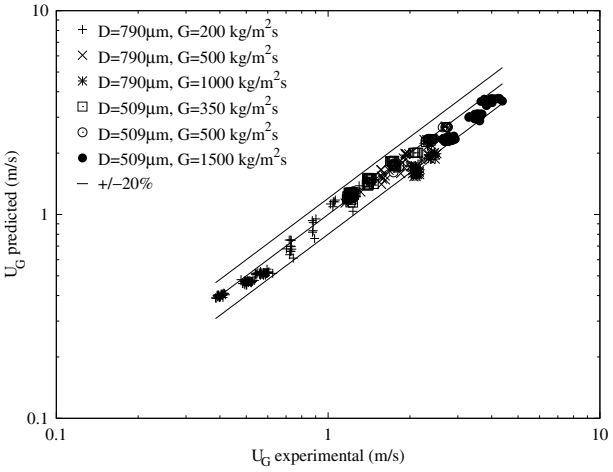


Fig. 11. Comparison between the experimental vapor velocity and that predicted by the model with 90% of the data predicted within a ±20% error band.

$$\text{MAE} = \frac{1}{N}\sum_{1}^{N}\left|\frac{\text{experimental value} - \text{predicted value}}{\text{experimental value}}\right| \times 100 \quad (42)$$

$$\text{ME} = \frac{1}{N}\sum_{1}^{N}\left(\frac{\text{experimental value} - \text{predicted value}}{\text{experimental value}}\right) \times 100 \quad (43)$$

Fig. 12 shows the comparison between the experimental data and the model for 509 and 709 µm tube diameter and a mass flux of 500 kg/m² s. The agreement is quite good. Here it can be noted that the larger the diameter, the higher the vapor velocity. The model correctly captures this trend. The vapor velocity increases with the vapor bubble length and then reaches a plateau. This variation explains the reason for the collision of the elongated

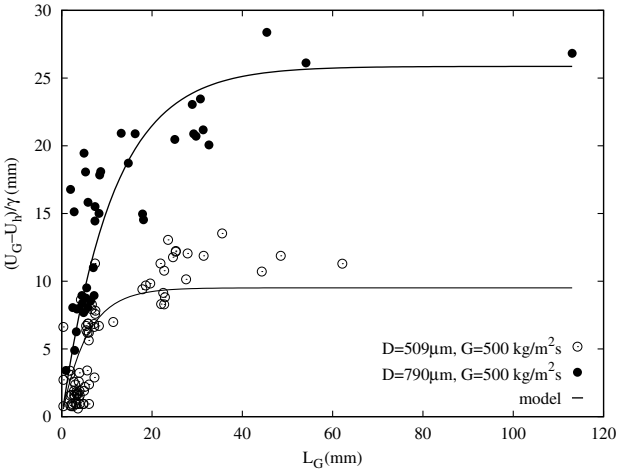


Fig. 12. Comparison between the experimental relative vapor velocities and the model for R-134a, $D = 0.509$ and 0.790 mm and $G = 500$ kg/m² s.

bubbles in microchannels. A "long" elongated bubble travels faster than a shorter one ahead of it and will reach it downstream. When all the bubbles have a certain length, represented here by the plateau, the vapor velocity does not change anymore and bubble collision will no longer occur, i.e. the flow becomes fully developed.

Using the above model to predict the mean vapor velocity of an elongated bubble in a microchannel, it is possible use this velocity to calculate the corresponding void fraction $\epsilon$ using the following equation:

$$\epsilon = \frac{j_G}{U_G} = \frac{G \cdot x/\rho_G}{U_G} \tag{44}$$

with $j_G$ the vapor superficial velocity. The void fraction was calculated as a function of vapor quality, for R-134a at $T_{sat} = 30$ °C, $G = 1000$ kg/m$^2$ s, in a 0.509 mm diameter tube and for three hypothetical average bubble lengths: 1, 10 and 100 mm. These values are plotted in Fig. 13, showing the homogeneous and Zivi void fraction as the reference. Also plotted are the void fractions obtained indirectly for similar test conditions (but not able to be done simultaneously) using a cross-correlation of two laser light signals to obtain elongated bubble velocities described in Revellin et al. (2006). For vapor qualities less than 0.05 and $L = 1$ mm, i.e. typically bubbly flow, the two independent measurement techniques are shown to provide good agreement with the homogeneous model. For vapor qualities larger than 0.05, the void fraction measured with the laser technique departs from the homogeneous model and is close to the void fraction calculated with an average bubble length of 10 mm, typically an elongated bubble flow pattern. If the model is extrapolated up to a vapor quality of 0.25, logically the void fraction calculated with an average bubble length of 100 mm tends towards the Zivi model, which is valid for annular flow.

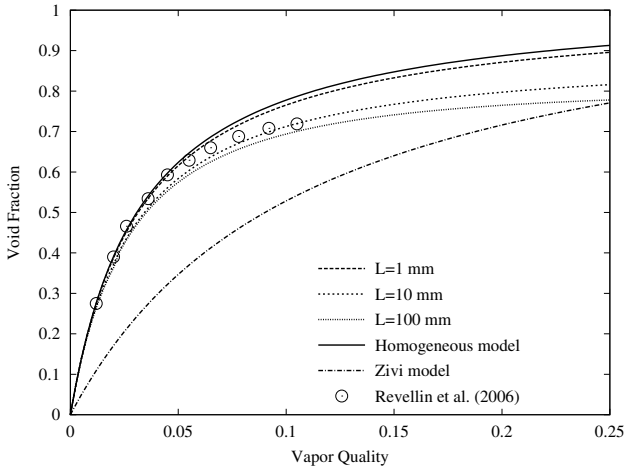


Fig. 13. Comparison between the homogeneous and Zivi model, Revellin et al. (2006) indirect void fraction measurements, and the void fraction predicted by Eq. (46) (R-134a, $D = 0.509$ mm, $G = 1000$ kg/m$^2$ s and $T_{sat} = 30$ °C), for three lengths of bubbles.

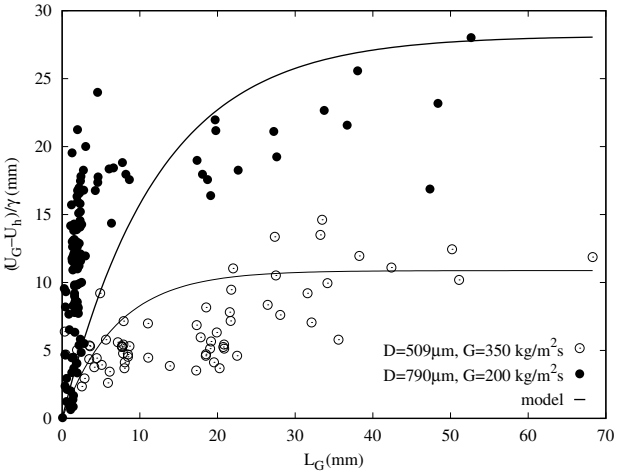


Fig. 14. Comparison between the experimental relative vapor velocities and the model for R-134a, $D = 0.509$ mm, $G = 350$ kg/m$^2$ s and $D = 0.790$, $G = 200$ kg/m$^2$ s.

Fig. 14 shows the comparison between the experimental data and the model for 509 and 709 μm tube diameters at mass fluxes, respectively, of 350 and 200 kg/m$^2$ s. The agreement between the data and the model is also reasonably good.

## 6. Results and discussion

Some simulations were performed with this model to outline the different trends of the elongated bubble velocity. In each case the vapor quality was kept constant at 10%.

The simulation of the influence of the diameter $D$ on the relative bubble velocity $U_G - U_h$ and the length of the elongated bubble is shown in Fig. 15. The mass velocity and saturation temperature were fixed at 500 kg/m$^2$ s and 30 °C, respectively. The larger the diameter, the higher

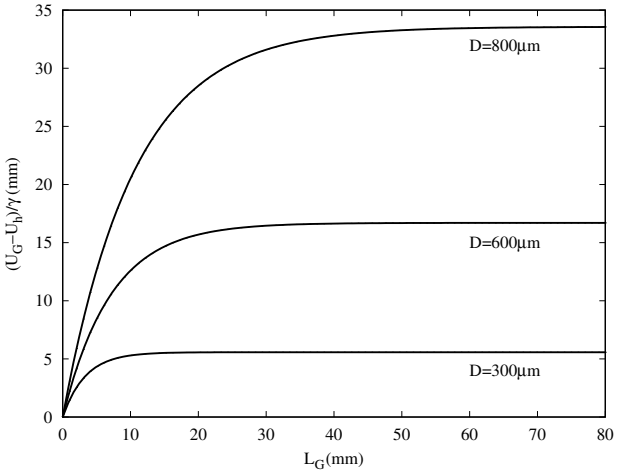


Fig. 15. Simulation of the influence of the diameter $D$ on the relative bubble velocity as a function of the elongated bubble length for R-134a, $T_{sat} = 30$ °C, $L_{MEV} = 70$ mm, $x_{MEV,out} = 0.1$ and $G = 500$ kg/m$^2$ s.

the relative bubble velocity, and the faster the increase of $U_G - U_h$, as also evident in the present experimental data. This is consistent with an increasing interaction of the vapor and liquid phases when the diameter decreases. This effect probably occurs as long as the bubbles are confined. Notably this means that if the diameter is small enough, the relative elongated bubble velocity is negligible and the homogeneous model prevails. This conclusion is supported by Serizawa et al. (2002) and Serizawa and Kawara (2003) who observed that the void fraction was reasonably well predicted by the homogeneous model for air–water flow in circular tubes of 20, 25 and 100 μm internal diameter and for steam-water flow in a 50 μm internal diameter tube.

Fig. 16 shows the simulation of the influence of the mass velocity $G$ on the relative bubble velocity $U^*$ and the length of the elongated bubble. The tube diameter and saturation temperature were fixed at 500 μm and 30 °C, respectively. The larger the mass velocity, the higher the relative bubble velocity, and the earlier the increase of $U_G - U_h$, as noticed in the present experimental data. This conclusion is supported by Revellin (2005) and Revellin et al. (2006) who measured the same effect with cross-correlations applied on signals from two pairs of lasers and diodes to detect bubble velocities of R-134a at the exit of an evaporator.

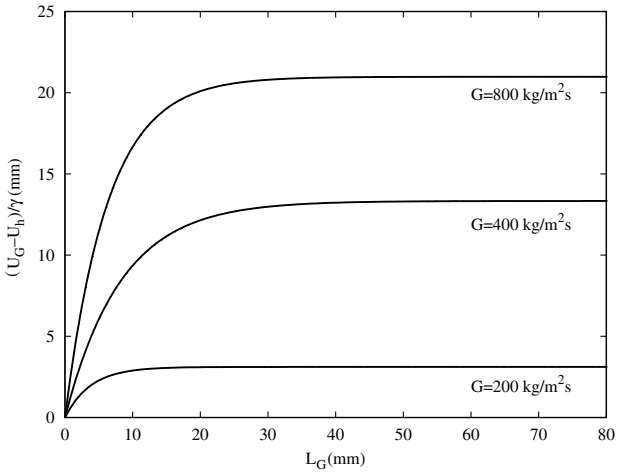


Fig. 16. Simulation of the influence of the mass velocity $G$ on the relative bubble velocity as a function of the elongated bubble length for R-134a, $T_{sat} = 30$ °C, $L_{MEV} = 70$ mm, $x_{MEV,out} = 0.1$ and $D = 500$ μm.

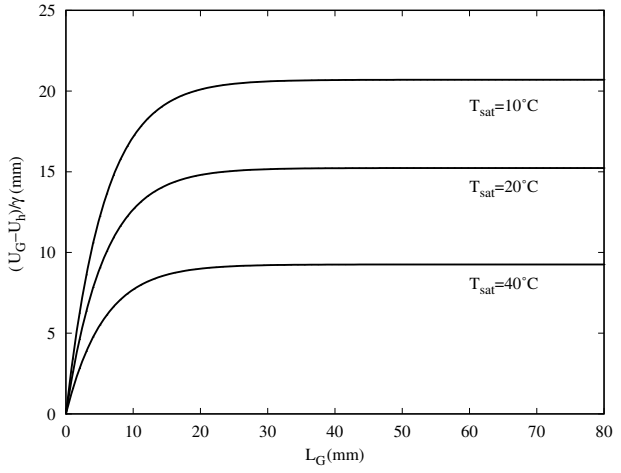


Fig. 17. Simulation of the influence of the saturation temperature $T_{sat}$ on the relative bubble velocity as a function of the elongated bubble length for R-134a, $D = 500$ μm, $L_{MEV} = 70$ mm, $x_{MEV,out} = 0.1$ and $G = 500$ kg/m$^2$ s.

Fig. 17 shows the simulation of the influence of the saturation temperature $T_{sat}$ on the relative bubble velocity $U^*$ and the length of the elongated bubble. The tube diameter and mass velocity were fixed at 500 μm and 500 kg/m$^2$ s, respectively. The higher the saturation temperature (and hence the pressure), the lower the relative bubble velocity, and the smaller the increase of $U_G - U_h$. This effect could not be experimentally verified with the present data since only one saturation temperature was tested and is thus an extrapolation of the model. However, this is consistent with the fact that with increasing pressure the difference between vapor and liquid densities decreases and thus the velocity difference between the vapor and liquid phases decreases so that the homogeneous model prevails at high pressure.

## 7. Conclusions

The velocity of elongated vapor bubbles exiting two horizontal micro-evaporator channels with refrigerant R-134a was studied. Experimental data with tube diameters of 509 and 790 μm, mass velocities from 200 to 1500 kg/m$^2$ s, vapor qualities from 2% to 19% and a saturation temperature of 30 °C were analyzed with a fast digital camera. It was shown experimentally that the relative elongated bubble velocity increased with increasing bubble length until a plateau was reached, and also increased with increasing diameter and mass velocity. Furthermore, an analytical model developed for a diabatic two-phase flow, was devised that was able to predict all of these different trends. An extrapolation of the model predicts that the relative elongated bubble velocity should decrease with increasing pressure, which is consistent with the physics of two-phase flow. In future work this model can be used to predict the bubble collision phenomena. For a given distribution of elongated bubble lengths, the new distribution after a given time delay can be calculated and eventually the transition between slug and annular flow could be predicted.

## Acknowledgements

B. Agostini is supported by the Swiss Confederation under the CTI-project No. 6862.2 DCS-NM.

R. Revellin is supported by the Swiss National Science Foundation (SFN) Grant number 20 111626/1.

## References


Barnea, D., Taitel, Y., 1993. A model for slug length distribution in gas–liquid flow. Int. J. Mulitphase flow 19, 829–838.

Cook, M., Behnia, M., 2000. Slug length prediction in near horizontal gas–liquid intermittent flow. Chem. Eng. Sci. 55, 2009–2018.

Cornwell, K., Kew, P.A., 1995. Evaporation in microchannel heat exchangers. In: Proceedings 4th UK National Conference on Heat Transfer. Manchester, U.K., pp. 289–294.

Kashid, M.N., Gerlach, I., Goetz, S., Franzke, J., Acker, J.F., Platte, F., Agar, D.W., Turek, S., 2005. Internal circulation within the liquid slugs of liquid–liquid slug flow capillary microreactor. Indus. Eng. Chem. Res. 44, 5003–5010.

Kew, P.A., Cornwell, K., 1997. Correlations for the prediction of boiling heat transfer in small-diameter channels. Appl. Therm. Eng. 17, 705–715.

Pinto, A.M.F.R., Pinheiro, M.N.C., Campos, J.B.L.M., 1998. Coalescence of two gas slugs rising in a co-current flowing liquid in vertical tubes. Chem. Eng. Sci. 53, 2973–2983.

Revellin, R., 2005. Experimental two-phase fluid flow in microchannels. Ph.D. Thesis. Ecole polytechnique Fédérale de Lausanne, <http://library.epfl.ch/en/theses/?nr=3437/>.

Revellin, R., Dupont, V., Ursenbacher, T., Thome, J.R., Zun, I., 2006. Characterization of diabatic two-phase flows in microchannels: flow parameter results for R-134a in a 0. 5 mm channel. Int. J. Multiphase Flow 32, 755–774.

Revellin, R., Thome, J., 2006. New diabatic flow pattern map for evaporating flow in microchannels. In: Proceedings of the 13th International Heat Transfer Conference. Sydney, Australia.

Ribatski, G., Wojtan, L., Thome, J., 2006. An analysis of experimental data and prediction methods for two-phase frictional pressure drop and flow boiling heat transfer in microscale channels. etfsIn Press.

Serizawa, A., Kawara, Z., 2003. Fluid-dynamic characteristics of two-phase flow in microchannels. In: The 10th International Topical Meeting on Nuclear Reactor Thermal Hydraulics (NURETH-10). October 5–9, Seoul, Korea.

Serizawa, A., Kunugi, T., Kawara, Z., Takahashi, O., 2002. Two-phase flow in microchannels. In: Fourth pacific Rim Thermal Science and Energy Engineering Workshop. May 31–June 2, Kyoto, Japan, pp. 136–141.

Talvy, C.A., Schemer, L., Barnea, D., 2000. On the interaction between two consecutive elongated bubbles in a vertical pipe. Int. J. Multiphase Flow 26, 1905–1923.

Thome, J.R., Dupont, V., Jacobi, A.M., 2004. Heat transfer model for evaporation in micochannels. Part 1. Presentation of the model. Int. J. Heat Mass Transfer 47, 3375–3385.

Ullman, A., Brauner, N., 2006. The prediction of flow pattern maps in minichannels. In: 4th Japanese-European Two-Phase Flow Group Meeting. 24–28 September, Kyoto, Japan.

Yang, Z.L., Palm, B., Sehgal, B.R., 2002. Numerical simulation of bubbly two-phase flow in a narrow channel. Int. J. Heat Mass Transfer 45, 631–639.

Zuber, N., Findlay, J.A., 1965. Average volumetric concentration in two-phase flow systems. J. Heat Transfer 87, 458–463.